

Color Space Conversion via Gamut-Based Color Samples of Printer

Cheol-Hee Lee,^{▲,*} Eung-Joo Lee,[†] Suk-Chul Ahn,^{▲,‡} and Yeong-Ho Ha^{▲,§}

^{*}Department of Computer Engineering, Kyungwoon University, Kumi, Kyungbuk, Korea

[†]Dept. of Information/Communication Engineering, Tongmyong University of Info. Tech., Pusan, Korea

[‡]Division of Image and Information Engineering, Pukyong National University, Pusan, Korea

[§]School of Electronic and Electrical Engineering, Kyungpook National University, Taegu, Korea

Because many types of electronic imaging devices are now available, cross-media color reproduction technology has received widespread attention due to the need to provide accurate color stimuli for different devices. In the case of cross-media color reproduction between a monitor and a printer, RGB has to be converted into a device-independent color space in order to translate the color information between the two devices. Thereafter, gamut mapping is used to compensate for any gamut mismatch and device-independent colors have to be re-converted into output colors such as CMY control values for printing. For color conversion between device colors and device-independent colors, empirical representation using sample measurements is currently widely utilized. In the case of the printer, color samples are uniformly selected in the colorant space, printed as color patches, and then measured. However, because these color samples are not evenly distributed inside the printer gamut, the color conversion error is increased. Accordingly, this article introduces a color-sampling algorithm for a printer to reduce the error in color conversion, and the performance is analyzed via color conversion experiments using three conversion methods, regression, neural network, and interpolation.

Journal of Imaging Science and Technology 45: 427–435 (2001)

Introduction

Many types of electronic imaging devices are currently available, including color cathode ray tube (CRT) devices, ink jet printers, offset printing devices, thermal transfer printers, and all of these devices utilize device-dependent color spaces for color specification. However, device-dependent color spaces do not relate to an objective definition of color or human color perception. Therefore, CIE developed device-independent color spaces to give a quantitative measure for all colors that is not dependent on the imaging device. As a result, the production of color consistency between various devices, that is, the concept of device-independent color reproduction, has received widespread attention. Device-independent color reproduction requires a color conversion between device colors and device-independent colors, specified by the standard color space like the CIEL*a*b* color system to achieve color consistency.

Color reproduction on a CRT monitor is based on an additive mixture of three primaries, for which the color space conversion is usually performed with a 1-dimensional nonlinear mapping and matrix transformation. In contrast, color reproduction in a printer is based on a subtractive mixture of either three primaries, Cyan (C), Magenta (M), and Yellow (Y), or four with the inclusion of Black (K). However, the color stimulus generated on

paper is usually quite difficult to predict when only based on amounts of ink for these primaries. In other words, because of the complicated nonlinear relationship between the device-dependent input and the device-independent output signals of a printer, it is difficult to control the CMYK color signals in an 1-dimensional nonlinear mapping followed by multiplication with a matrix.

Several methods have been proposed for estimating the amounts of primary inks necessary to produce a desired color stimulus. These include an analytical method using the Neugebauer equations,¹ the polynomial regression model,^{2–5} 3-dimensional interpolation using a look-up table (LUT),^{6–10} and neural network methods.^{11–13} The analytical model involves a prediction that uses several device measurements, however, this method suffers from an inevitable discrepancy between printer outputs because the analytical methods are not accurate enough due to the many disturbance elements in real printer systems. In the polynomial regression method, a system is assumed to be a black box and the parameters are obtained from the input–output relationships. Three-dimensional interpolation creates a data table of measured color values and then interpolates this table to determine the input signal for generating a desired color output. Neural network methods model the mapping between the printer color signal and the output color stimulus values using pre-determined weighting factors. When compared to the analytical method using Neugebauer equations, the regression, neural network, and LUT conversion methods all produce a high accuracy in color conversion. In these methods, a device is regarded as an unknown static system, and its input–output relationship is modeled using input values and

Original manuscript received June 5, 2000

▲ IS&T Member

©2001, IS&T—The Society for Imaging Science and Technology

the corresponding measured values of color patches. Accordingly, the selection of color samples is very important to reduce the estimation error. For example, if the size of the color samples is small, a color discrepancy will inevitably occur, plus if the distribution of the color samples is not uniform, the deviation of the estimation error will also increase.

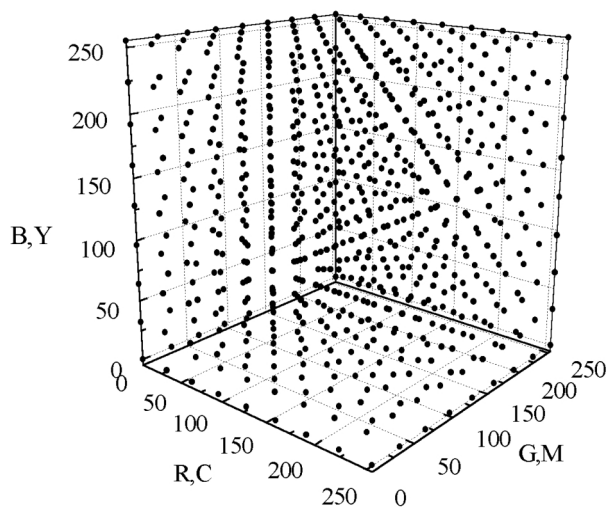
In the conventional approach for printers, color samples are uniformly selected in a colorant space. Through printing the selected color control signals, color patches are then generated and measured to produce the corresponding output signals in terms of CIEL*a*b*. However, in the case of conventional uniform sampling in CMY colorant space, there is a very non-uniform distribution of the color samples in CIEL*a*b* space, required for making decisions on the best color compromise for device-dependent color reproduction, that concentrates on the low lightness axis due to a dot-overlap and dot gain. Therefore, for the effective modeling of a printer system, uniform color samples in CIEL*a*b* space are required that will fit a printer gamut.

To model a printer gamut, the gamut boundary needs to be calculated. In this study, the printer gamut is determined using 3 primaries, 3 secondaries, and black. Next the initial sample points are uniformly distributed among grid points of divided cubes in CIEL*a*b* space. Thereafter, a fixed size of uniform sample points is generated from the initial sample points by removing the outside grid points. However, although these uniform sample points represent uniform position information in a CIEL*a*b* printer gamut, the corresponding input driving signals of CMY must also be calculated to generate real uniform color sample patches. A multi-layered perceptron¹⁴ with a 3–100–3 structure is utilized to estimate the CMY control signals of the uniform sample points. Finally, the CMY values for the uniform sample points are printed and measured using a colorimeter, and these input–output pairs of gamut-based color samples are then used to model the printer system.

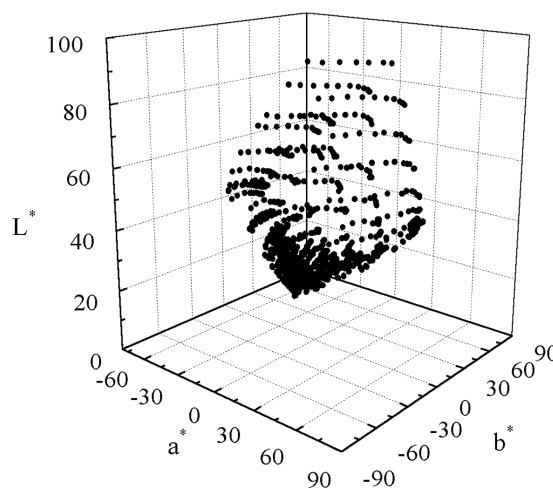
Determination of Color Samples Based on Printer Gamut

A color output device can be represented as a mapping function between a set of digital control values and colors specified in a device-independent color space. Figures 1(b) and 1(c) show the color specifications in CIEL*a*b* space for digital control values of Fig. 1(a), which represents uniform 9 × 9 color samples in RGB and CMY space, respectively. As shown in Fig. 1b and 1c, the monitor and printer output colors relative to uniform control values are not uniform in CIEL*a*b* space and, in particular, the printer colors are strongly concentrated in the low lightness region.

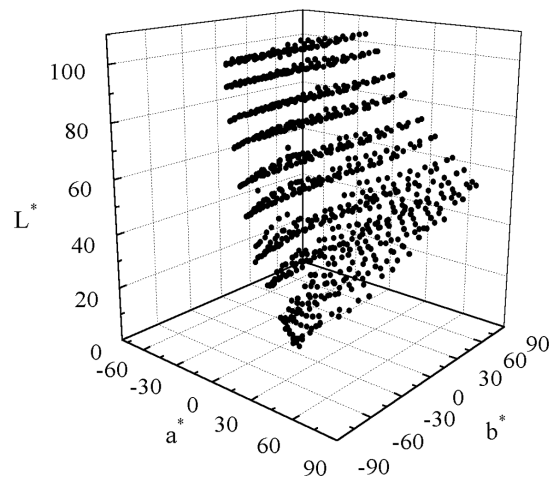
In an ink jet printer, the shape of printed ink droplets is almost circular. Accordingly, these dots have to be overlapped in order to print over the entire area of the printing material. However, printed dots have additional dot growth problem referred to as dot gain depending on ink, paper grade and viewing conditions. There are two types of dot gain. One is mechanical dot gain, which is a physical enlargement of the printed dot, and the other is optical dot gain, which is an apparent visual enlargement due to an interaction between light and the paper substrate in the vicinity of the dot.¹⁵ These facts cause lightness reduction and makes reproduced colors much darker than they should be. Therefore, in order to model a printer gamut effectively, it is important to select color samples that are uniformly distributed throughout the entire printer gamut.



(a)



(b)



(c)

Figure 1. Uniform digital control values of printer and monitor and their corresponding specifications in CIEL*a*b* space; (a) is uniformly sampled monitor and printer colors in RGB and CMY space, respectively, (b) is measured printer outputs in terms of CIEL*a*b*, and (c) is measured monitor outputs in terms of CIEL*a*b*.

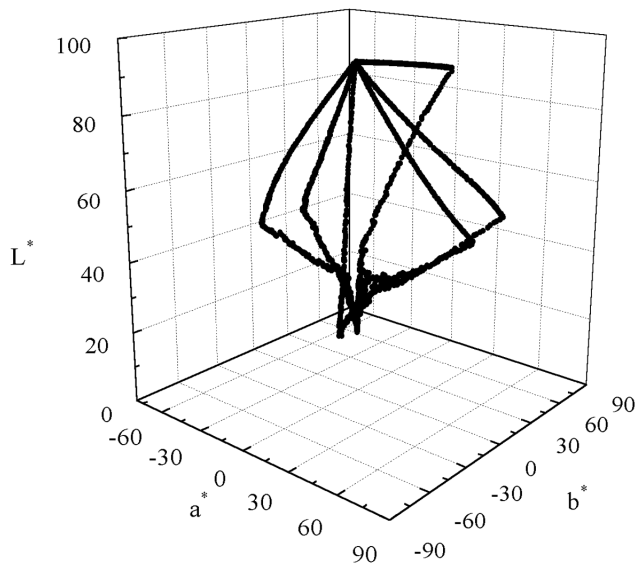


Figure 2. Gamut volume represented by primary colors.

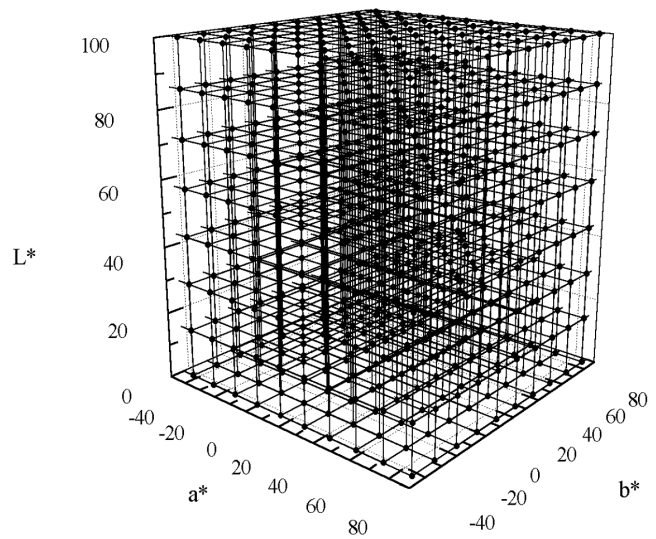


Figure 3. Allotment of initial sample points in CIEL*a*b* space.

Determination of Gamut Volume

The gamut volume of a printer can be assessed differently according to the dot allocation method used in the dithering process. However, in the current approach a printer is assumed to be a static system and its gamut is estimated using the fixed halftoning method.

Figure 2 shows the gamut volume of a printer assessed using C, M, Y, R, G, B, and K primary colors and the halftone pattern of a blue noise mask.¹⁶ For each primary color, 256 color patches were generated and their reproduced colors were then measured with a colorimeter to obtain the corresponding CIEL*a*b* specifications.

Allotment of Initial Sample Points

After determining the gamut boundary, the initial sample points are uniformly allotted in the gamut to model the gamut volume. For uniform sampling in a CIEL*a*b* printer gamut, the gamut volume is divided into a set of cubes. Figure 3 shows the divided sub-cubes and their vertices in a CIEL*a*b* printer gamut. In this figure, the lightness distribution is from 28.4179 to 93.6327 and the hue range is from -53.7799 to 75.5809 and from -52.9612 to 86.2676 for a^* and b^* , respectively. These values were obtained based on gamut measurements with primary colors of Fig. 2 and utilized to limit the gamut range when allotting the initial sample points.

As the size of the cubes decreases, a detailed gamut representation becomes possible. However, large-sized samples require a lot of time in color space conversion. In this study, the side length of each cube was arbitrary set at 7.0921, thereby dividing the lightness into 14 levels with a total of 3049 vertices.

Selection of Sample Points Included In Printer Gamut

For uniform sampling, the initial sample points were distributed among the vertices of the divided cubes in a limited CIEL*a*b* cube. However, some of the initial sample points may also be outside the printer gamut, as shown in comparison of Figs. 2 and 3. To model the printer gamut of Fig. 2, those sample points located outside the gamut need to be excluded. In this research, the decision, related to including sample points is calculated based on a volume comparison with tetrahedra.

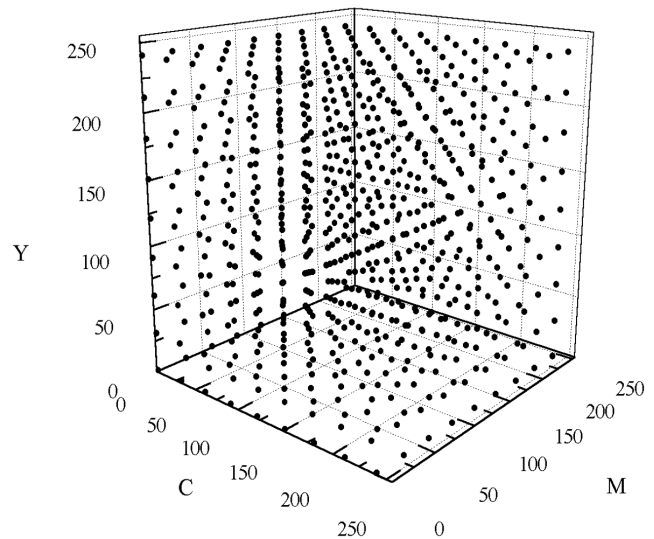


Figure 4. CMY control signals, uniformly distributed in colorant space.

Figure 4 shows the distribution of a CMY control signal for a gamut measurement including inside the printer gamut.

In Fig. 4, each vertex of a cube has a CMY value of the device input space and its corresponding measured $L^*a^*b^*$. As shown in Fig. 4, $9 \times 9 \times 9$ CMY sample patches were generated and measured for gamut measurements. Then, all the cubes were divided into six tetrahedra to generate look-up tables for the gamut. This tetrahedral division technique is quoted from Ref. 10.

Each element of the look-up tables represents a tetrahedron and has measured $L^*a^*b^*$ values for the four vertices of each tetrahedron. After composing look-up tables for all tetrahedra, each initial sample point in Fig. 3 is compared to all the elements in the look-up tables using barycentric interpolation coefficients in

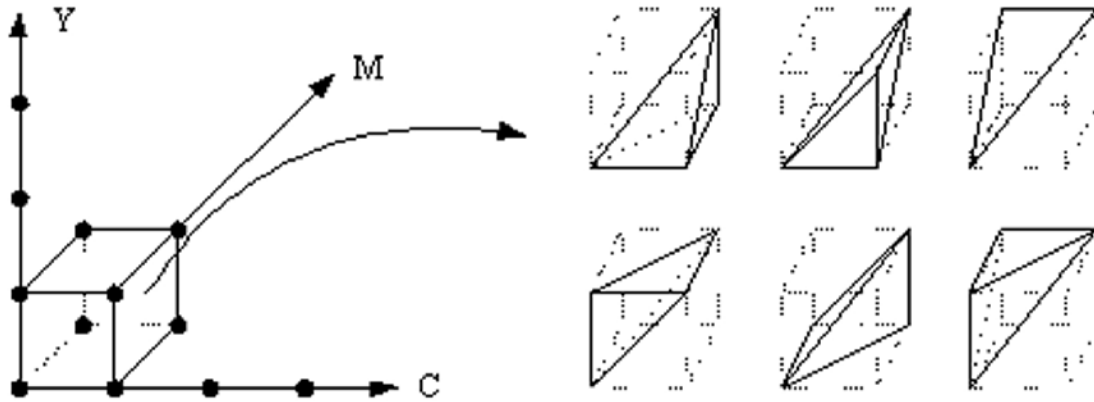


Figure 5. Tetrahedral division of a subcube.

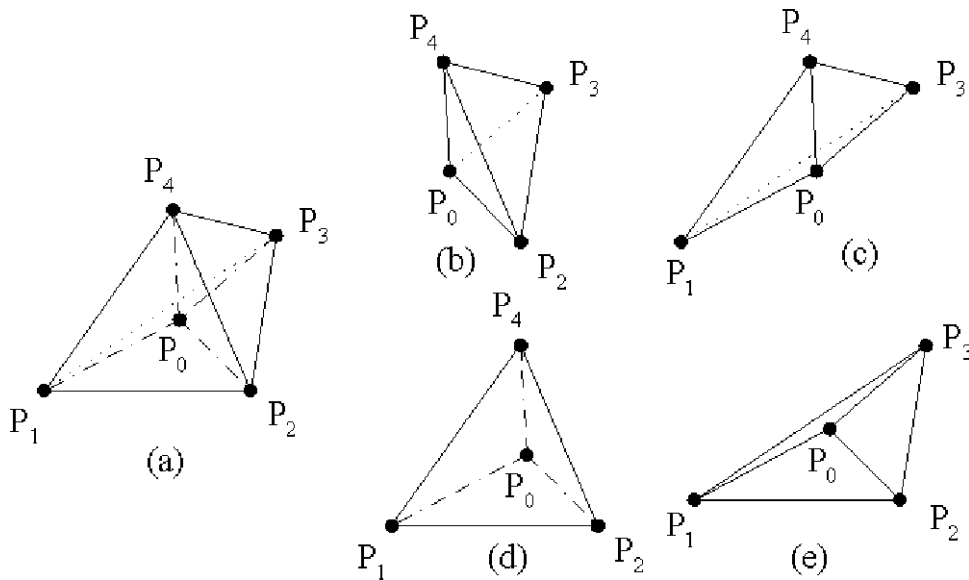


Figure 6. Partition of a tetrahedron for volume comparison; (a) is a tetrahedron, (b),(c),(d), and (e) is sub-tetrahedra of (a).

order to determine whether the current sample point is included within the printer gamut, quoted in Ref. 17.

In Fig. 6, p_0 represents an initial sample point of Fig. 3 with $L^*a^*b^*$ specifications, and p_1, p_2, p_3 and p_4 represent the stored $L^*a^*b^*$ values of each tetrahedron in the look-up tables. These values are measured data for each grid point of Fig. 4. As shown in Fig. 6, each tetrahedron in the look-up tables is divided into four sub-tetrahedra. Next, when the volume of the tetrahedron (a) is defined as V_T and the volumes of the (b), (c), (d), and (e) sub-tetrahedra are set at V_1, V_2, V_3 and V_4 , respectively, the volume of each tetrahedron can be calculated by the equation below.

$$\begin{aligned}
 V_T &= \frac{1}{6} \begin{vmatrix} p_1 & p_2 & p_3 & p_4 \\ 1 & 1 & 1 & 1 \end{vmatrix}, & V_1 &= \frac{1}{6} \begin{vmatrix} p_0 & p_2 & p_3 & p_4 \\ 1 & 1 & 1 & 1 \end{vmatrix} \\
 V_2 &= \frac{1}{6} \begin{vmatrix} p_1 & p_0 & p_3 & p_4 \\ 1 & 1 & 1 & 1 \end{vmatrix}, & V_3 &= \frac{1}{6} \begin{vmatrix} p_1 & p_2 & p_0 & p_4 \\ 1 & 1 & 1 & 1 \end{vmatrix}, & (1) \\
 V_4 &= \frac{1}{6} \begin{vmatrix} p_1 & p_2 & p_3 & p_0 \\ 1 & 1 & 1 & 1 \end{vmatrix},
 \end{aligned}$$

where, $|\cdot|$ denotes the determinant. If an initial sample point is included into printer gamut, the sample point will have more than one tetrahedron, which satisfies the equation below.

$$\begin{aligned}
 W_i &\geq 0 \text{ and } W_1 + W_2 + W_3 + W_4 = 1, \quad i = 1, 2, 3, 4 \\
 W_i &= \frac{V_i}{V_T}, \quad i = 1, 2, 3, 4
 \end{aligned} \quad (2)$$

That is, if an initial sample point is located inside a tetrahedron, the number of elements in the look-up tables satisfying Eq. 2, will be one, whereas if the sample point is placed at a vertex of a tetrahedron or on a boundary surface, the number of satisfying elements will be more than one. Accordingly, an initial sample point is not included within the printer gamut, if there are no elements in the look-up tables that satisfy Eq. 2. Thus by using barycentric interpolation coefficients, the sample points, located within the printer gamut can be chosen as uniform sample points to model printer gamut. Finally, Fig. 7 shows 3- and 2-dimensional distribution of 731 uniform sample points included within the printer gamut of CIEL^{*}a^{*}b^{*} space.

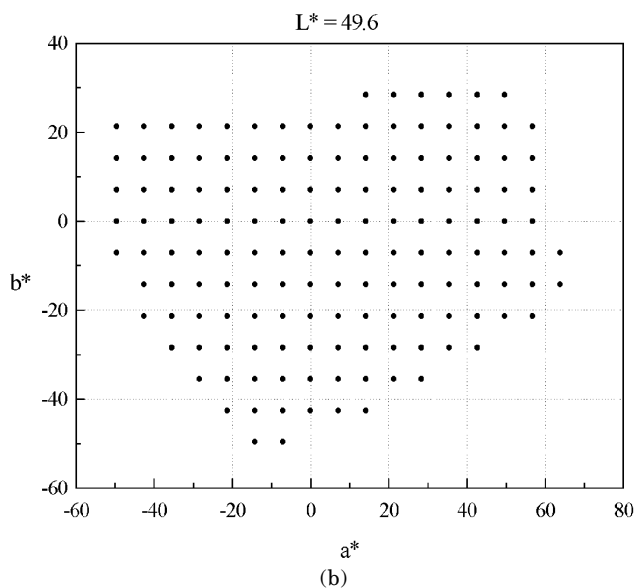
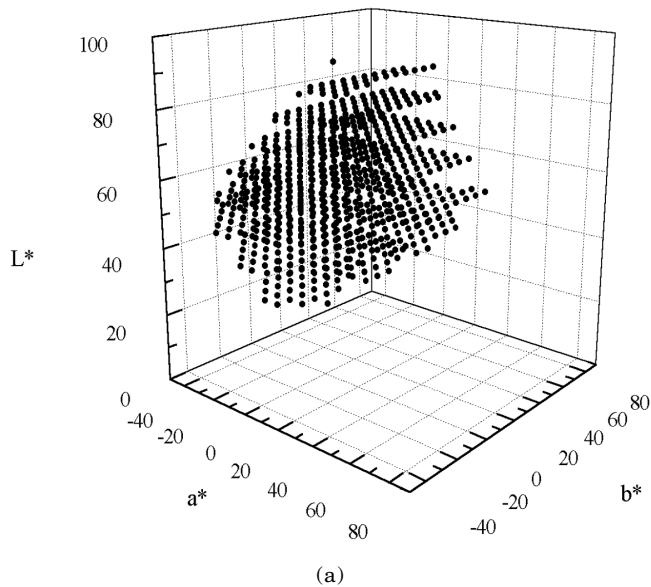


Figure 7. Graphical illustration of uniform sample points to model printer gamut; (a) 3-dimensional representation, (b) 2-dimensional representation on a^*b^* plane, given $L^* = 49.6$.

As mentioned earlier, the distribution of color samples, which are uniformly selected in CMY space, is highly related to lightness. Therefore, as the lightness is decreased, the distribution of the color samples becomes denser. This clustering phenomenon occurs with all ink jet printers. Moreover, if color stimuli are then predicted using these color samples, the prediction error will result a substantial difference inside the gamut volume and the total estimation error will also increase. In particular, the estimation error in the bright region of the gamut, which is very sensitive to color perception, will increase due to insufficient color samples as opposed to the dark region of the gamut. Consequently, when modeling the input–output relationship of an unknown printer system, the corresponding CMY values of the uniform sample points must be calculated. Therefore, to relate CMY with the CIEL^{*} a^*b^* uniform sample points, the color conversion of CIEL^{*} a^*b^* to CMY is required.

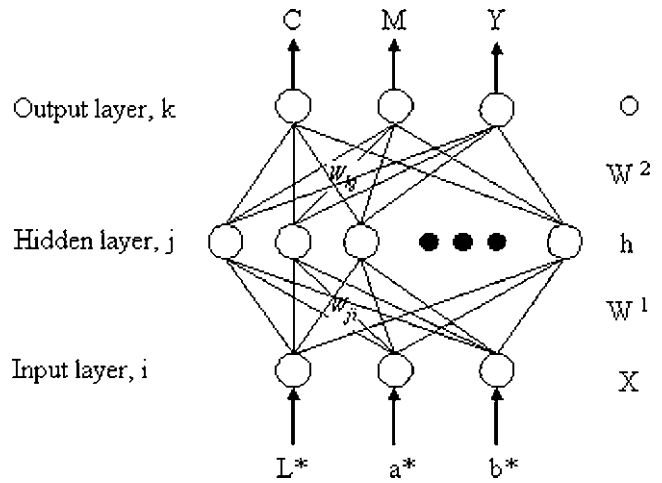


Figure 8. Multi-layered perceptron with 3–100–3 structure.

Estimation of CMY Control Signals of the Uniform Sample Points. Subtractive color mixing printers generate color stimuli by mixing CMY signals. Thus, in order to estimate the CMY control signals for the uniform sample points, inverse printer system has to be modeled. In this study, a multi-layered perceptron system¹⁴ was used for this purpose. The mapping from CIEL^{*} a^*b^* signals to CMY colorants was implemented using a multi-layered perceptron with a 3–100–3 structure. The network size was determined by empirically selecting effective numbers of hidden layers and units. As shown in Fig. 8, each unit receives its input signals from the previous layer, computes the weighted sum, and then outputs the unit’s level of activation by weighting this sum with a nonlinear function.

Thus, all units except for the input layer can be described by

$$o_j = f\left(\sum_i w_{ji}o_i + b_j\right) \quad (3)$$

where o_i is the output of the i_{th} unit in the previous layer, w_{ji} is the weighting coefficient to connect the i_{th} unit of the previous layer with the j_{th} unit, b_j is the bias term, and f is the sigmoidal activation function as shown below

$$f(x) = \frac{1}{1 + \exp^{-x}}. \quad (4)$$

This function can take any real number within the range $[0 \sim 1]$. Therefore, all input and output signals have to be scaled to the interval $[0 \sim 1]$. Figure 9 shows the maximum chroma of each primary color. From Fig. 9, it is assumed that a^* and b^* of the input CIEL^{*} a^*b^* values are given as $[-60 \sim 90]$, respectively, the L^* input values are from $[0 \sim 100]$, and the output values of the CMY signal lie within a range of $[0 \sim 255]$.

For network learning, CMY and the measured values of conventional color samples uniformly selected in CMY space were used. The total number of color patches was 729. Each digital control value of CMY was set to 0, 32, 64, 96, 128, 160, 192, 224, and 255 for uniform sampling in the colorant space. Using a training set of these

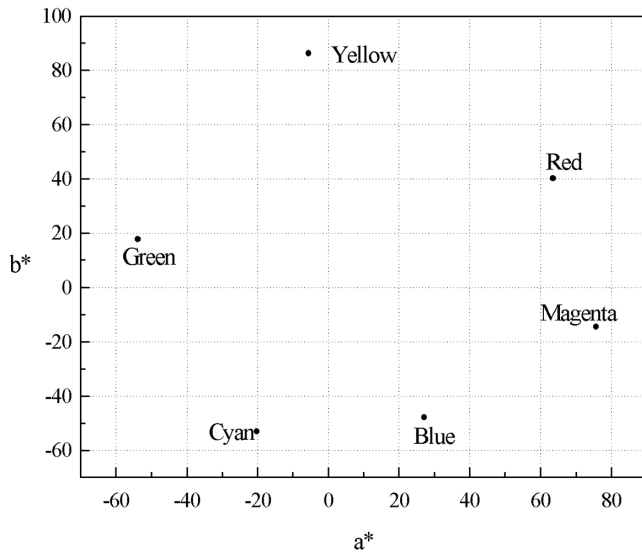


Figure 9. Maximum chroma of 3 primaries and 3 secondaries.

CIEL*a*b* and CMY pairs, back-propagation learning was performed to optimize the weights of the network, which were set at random values in the initial state. Figure 10 shows the transition of the total system error in the network learning.

The total system error can be represented as follows.

$$TSE = \frac{1}{2} \sum_{p=1}^{729} (t_p - o_p)^2 \quad (5)$$

where t_p are the scaled CMY values of the 729 color patches uniformly selected in colorant space and o_p are the output values of the network. After 3×10^6 iterations, the total system error was 0.163 and mean error per output node was 0.0004 for scaled data of [0 ~ 1].

A neural network should be able to generalize colors that are not included in the training set. For a generalization verification of the network, an additional 729 patches were generated. To exclude the CMY values, included in the training data, the training data CMY values were sub-sampled. The additional CMY values were 16, 48, 80, 112, 144, 176, 208, 240 and 1 was added for mapping the bright region. These CMY and CIEL*a*b* pairs were then used to test the network after network learning.

Table I shows the results for the 729 training data and the 729 test data for generalization. Max and Min represent the maximum and minimum difference between the estimated and real values, respectively. These CMY values were rescaled into a range of [0 – 255] for a comparison with the range of the original digital control values.

Generation of Proposed Gamut-Based Color Patches and Measurement

After determining the weights of the network, the proposed gamut-based printer samples are generated. In order to obtain the CIEL*a*b* and CMY data pairs of the proposed color samples, uniform sample points in terms of CIEL*a*b* are input into the neural system after back-propagation learning, then the output of the neural system, CMY values, are utilized as the printer

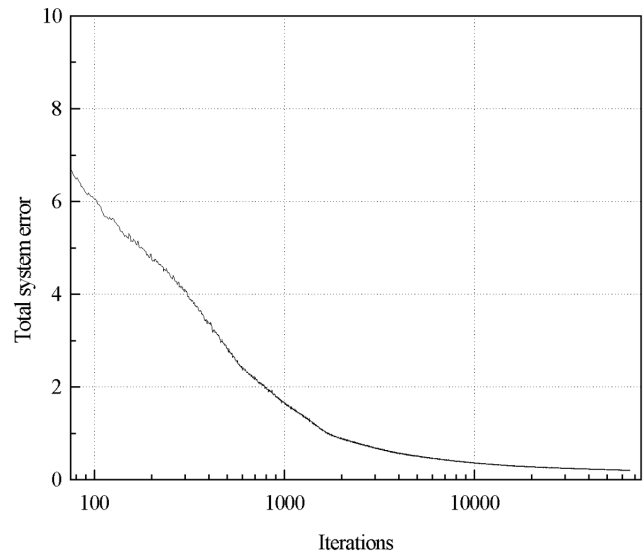


Figure 10. Total system error in iterative learning process of printer.

TABLE I. Generalization Test of Neural System

	729 training data		729 test data	
C [0–255]	Max	16	Max	20
	Min	0	Min	0
M [0–255]	Max	14	Max	16
	Min	0	Min	0
Y [0–255]	Max	7	Max	13
	Min	0	Min	0
Mean square error of CMY	2.5134		4.3455	

input signals. Figure 11(a) shows the network output namely, a gamut-based CMY control signal that generates the proposed gamut-based color samples, which are approximately uniform in CIEL*a*b* space. Figure 11(b) show the measured values of patches, generated by printer input of Fig. 11(a) in CIEL*a*b* space. Figure 11(c) represents the samples projected onto an a*b* plane when L* is from 48 to 50.

Compared to the fictive uniform sample points of Fig. 7(a) and (b), the proposed gamut-based samples are not completely uniform in printer gamut of CIEL*a*b* space due to estimation error in the color conversion with neural system and printer variability according to time and printing environments. However, the proposed sample points are comparatively uniform and independent to lightness.

Experiments

To evaluate the proposed color samples, color conversion experiments between the test chart and its reproduction were performed for neural network, regression, and interpolation methods, as shown in Fig. 12.

Fuji Color Paper IT8.7/2–1993 was utilized for the test chart. Figure 13 shows the distribution of the test chart color samples in CIEL*a*b* space.

First, a color space conversion experiment based on a neural network was simulated. A multi-layered

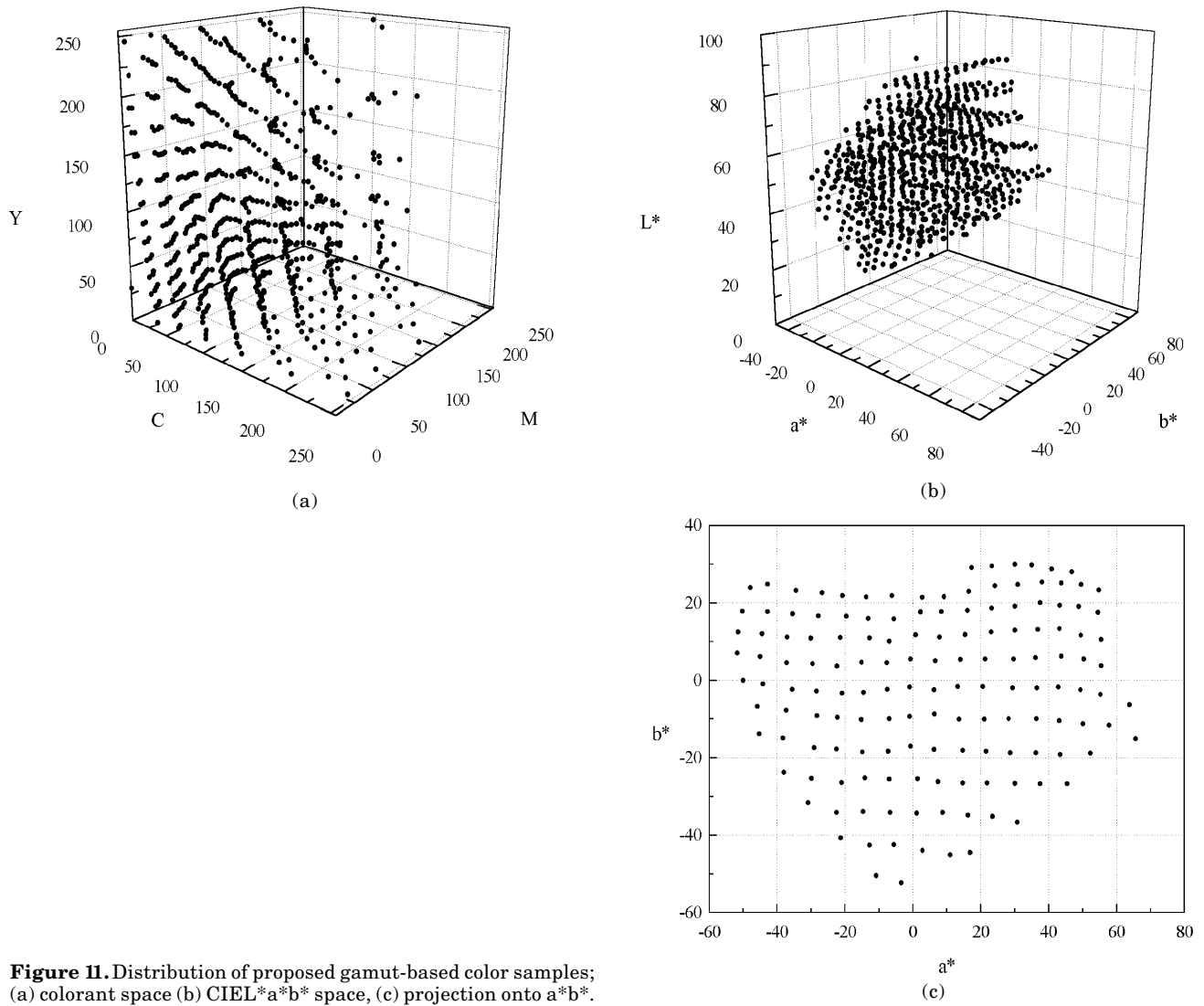


Figure 11. Distribution of proposed gamut-based color samples; (a) colorant space (b) CIE L*a*b* space, (c) projection onto a*b*.

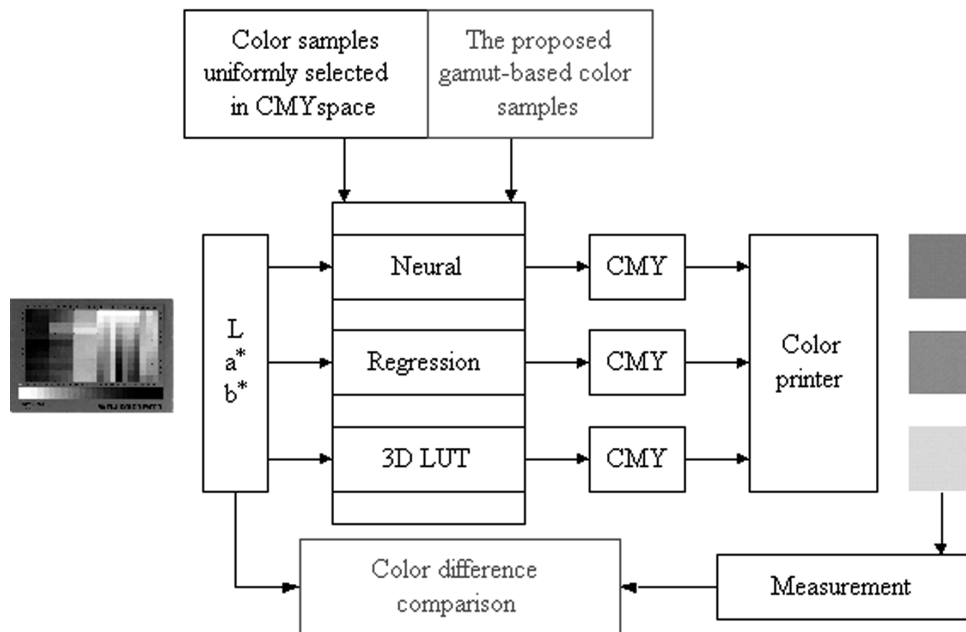


Figure 12. Color conversion experiment using test chart IT8.7/2-1993.

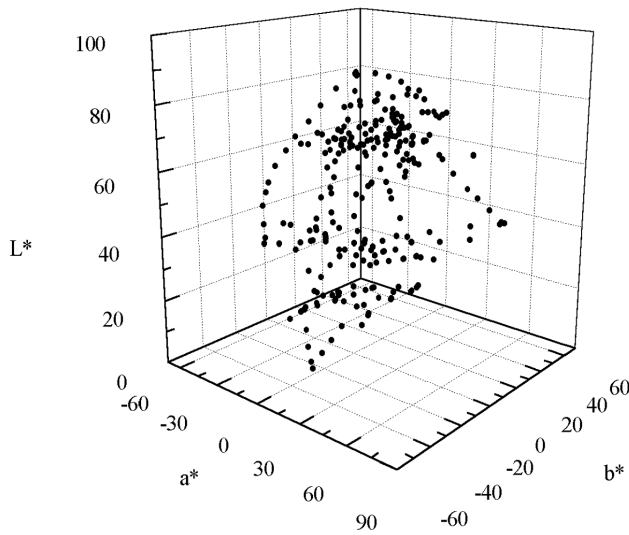


Figure 13. Distribution of IT8.7/2-1993 color samples in CIEL*a*b* space

perceptron network with a 3-100-3 structure, as in Fig. 8, was implemented and the weights for the uniform color samples in CMY space and the proposed gamut-based color samples were calculated, respectively. Here, the neural network input was scaled CIEL*a*b* values of the test charts and the network gave CMY control values within a range of [0 ~ 1]. Finally, the color patches were printed with re-scaled control values of [0 ~ 255] from the network output.

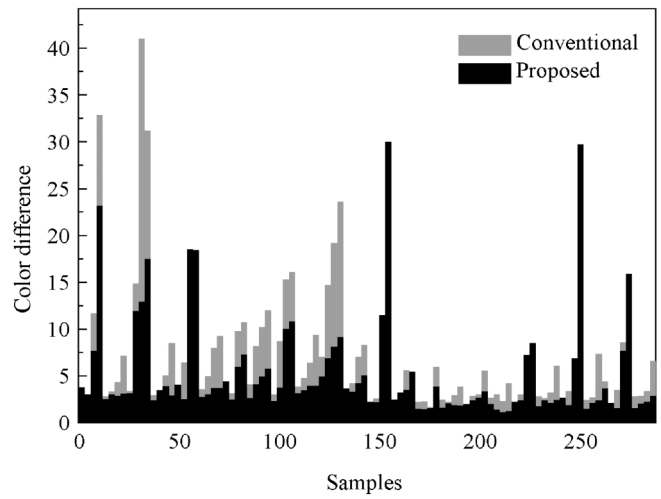
Second, a polynomial regression function was utilized for mapping the correlation between CIEL*a*b* and CMY using a multiple regression of 20 variables. Details of the implemented polynomial regression function can be found in Ref. 18. Two multiple regression functions of 20 variables were implemented using the 729 conventional color samples and 731 proposed gamut-based color samples, respectively.

Third, a 3-dimensional look-up table model using tetrahedral interpolation was also simulated for color conversion. This technique can be found in Ref. 10. Here, two look-up tables were generated for the 729 conventional color samples and 731 proposed color samples and exploited as mapping functions between CIEL*a*b* and CMY space.

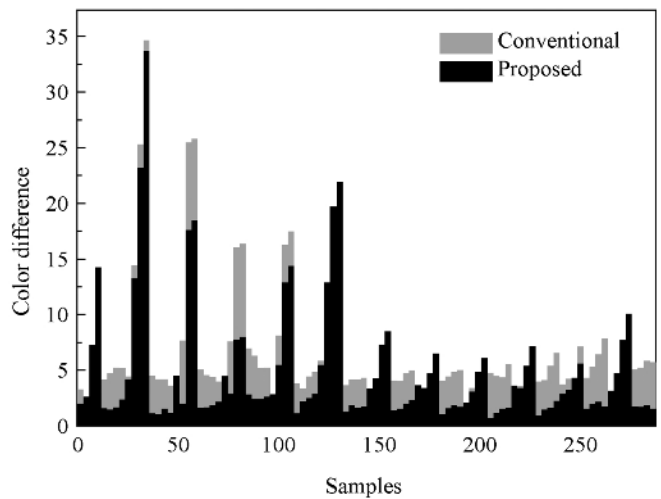
An ink jet printer was used to print the color patches. Blue-noise mask to generate halftone patterns of the test patches was utilized. For measurement of the sample colors of the test charts, a Techkon SP820 colorimeter was exploited. After the color conversion of the test charts using each color conversion method, modeled separately for two color samples, the color difference between the test charts and their reproductions for the three conversion methods was compared, as shown in Fig. 14.

Figure 14 shows resultant color difference for 264 Fuji color samples. As shown in Fig. 14, the proposed color samples produced a lower estimation error than the conventional color samples over almost all samples of Fuji color paper regardless of the conversion method. Table II shows the numerical results for the color difference.

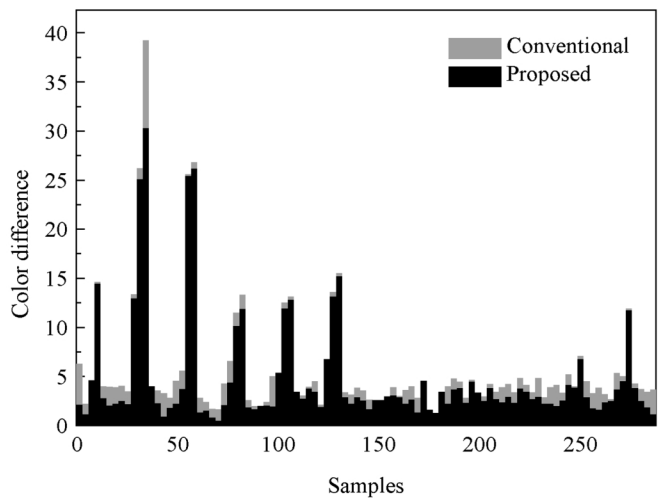
As shown in Table II, the mean and maximum color difference was reduced regardless of the color conversion method. In particular, the color difference was considerably reduced in the color conversion using



(a)



(b)



(c)

Figure 14. Color difference comparison; (a) neural network, (b) regression, and (c) interpolation.

TABLE II. Color Difference Comparison Relative To Color Conversion Method

Test chart	Color conversion method	Mean of color difference (Maximum color difference)	
		Color samples, uniformly selected in CMY space	Proposed gamut-based color samples
Fuji color paper (IT8.7/2-1993)	Regression	6.94 (16.25)	4.51 (15.11)
	Neural	5.38 (39.88)	3.89 (21.04)
	Interpolation	4.84 (40.23)	3.99 (21.72)

TABLE III. Color Difference Comparison For Color Samples Included In Printer Gamut

Test chart	Color conversion method	Mean of color difference (Maximum color difference)	
		Color samples, uniformly selected in CMY space	Proposed gamut-based color samples
Fuji color paper (IT8.7/2-1993)	Regression	5.83 (12.32)	2.89 (8.31)
	Neural	3.46 (10.73)	2.24 (10.30)
	Interpolation	2.99 (25.14)	2.29 (8.45)

regression. However, the maximum color difference was quite large because the test chart included many out-of-colors, not included in the ink jet printer gamut. Accordingly, a color conversion experiment using colors inside the printer gamut was simulated and the results are shown in Table III.

Conclusion

A color sample selection method was proposed to fit the gamut of a printer system in CIEL*a*b* space. To model a printer gamut, the gamut boundary needs to be calculated. In this study, the printer gamut was determined using 3 primaries, 3 secondaries, and black. Next the initial sample points uniformly allocated at the grid points of divided cubes in CIEL*a*b* space. Thereafter, a fixed size of uniform sample points was generated from the initial sample points by removing grid points of outside the printer gamut. However, because these uniform sample points are position data in CIEL*a*b* space, the corresponding CMY control signals were calculated to generate real color sample patches. A multi-layered perceptron with a 3-100-3 structure was utilized to estimate the CMY control signals of the uniform sample points. Finally, color patches were printed using the predicted CMY values for the proposed sample points and measured by a colorimeter, and these input-output pairs of gamut-based color samples were then used to model the printer system. To evaluate the performance of the proposed color samples, the color difference between a test chart and its reproduction was compared for the conventional and the proposed color samples. As a result, the proposed gamut-based color samples were able to reduce estimation error regardless of the color conversion method. The proposed method was particularly effective in color conversion when using the regression method. 

Acknowledgment. This work was supported by grant No.2000-1-30200-005-3 from the Basic Research Program of the Korea Science & Engineering Foundation.

References

1. G. L. Rogers, Neugebauer revisited: random dots in halftone screening, *Color Res. Appl.* **23**, 104-113 (1998).

2. M. Xia, E. Saber and A. M. Tekalp, End-to-end color printer calibration by total least squares regression, *IEEE Transactions on Image Processing*, **8**, 700-716 (1999).

3. H. R. Kang, Color technology for electronic imaging devices, SPIE Optical Engineering Press, Bellingham, WA, 1997, pp. 129-150.

4. H. R. Kang, Color scanner calibration, *J. Imaging Sci. Technol.* **36**, 162-170 (1992).

5. H. R. Kang, Color scanner calibration of reflected samples, *Proc. SPIE* **1670**, 468-477 (1992).

6. K. Knanmori, Fast color processor with programmable interpolation by small memory (PRISM), *J. Electronic Imaging* **2**, 213-224 (1993).

7. J. M. Kasson, S. I. Nin, W. Plouffe, and J. L. Hafner, Performing color space conversions with three-dimensional linear interpolation, *J. Electronic Imaging* **4**, 226-250 (1995).

8. K. Kanamori and H. Kotera, Color correction technique for hard Copies by 4 neighbors interpolation method, *J. Imaging Sci. Technol.* **36**, 73-78 (1992).

9. K. D. Genetten, RGB to CMYK conversion using 3D barycentric interpolation, *Proc. SPIE* **1909**, 117-123 (1993).

10. P. Hung, Colorimetric calibration in electronic imaging devices using a look-up table model and interpolations, *J. Electronic Imaging* **2**, 53-60 (1993).

11. S. Tominaga, Color control of printers by neural networks, *J. Electronic Imaging* **7**, 664-671 (1998).

12. Y. Arai, Y. Nakano and T. Iga, A method of transformation from CIEL*a*b* to CMY value by a three-layered neural network, *Proc. 1st IS&T/SID Color Imaging Conf.*, IS&T, Springfield, VA, 1993, pp. 173-177.

13. S. Tominaga, Color notation conversion by neural networks, *Color Res. Appl.* **18**, 253-259 (1993).

14. R. P. Lippmann, An introduction to computing with neural nets, *IEEE ASSP Magazine*, pp. 4-22 (Apr. 1987).

15. M. Wedin, Modeling of dot gain in halftone colour prints, Linköping Studies in Science and Technology Thesis no. 508, 1995, pp. 3.

16. T. Mitsa and K. J. Parker, Digital halftoning technique using a blue-noise mask, *J. Opt. Soc. Am. A* **9**, 1920-1929 (1992).

17. J. Y. Hardeberg and F. Schmitt, Color printer characterization using a computational geometry approach, *Proc. 5th IS&T/SID Color Imaging Conf.*, IS&T, Springfield, VA, 1997, pp. 96-99.

18. H. R. Kang, Color technology for electronic imaging devices, SPIE Optical Engineering Press, Bellingham, WA, 1997, pp. 55-62.

19. J. Chen and K. Huang, Adaptive color correction by high-order CMAC neural network, *Proc. of the 5th Color Imaging Conference*, IS&T, Springfield, VA, 1997, pp. 182-186.

20. Y. Lin and C. Lin, Color correction for printing devices with the use of neural networks, *Proc. of the 1998 Artificial Networks in Engineering Conf.*, vol. 8, St. Louis, MO, 1998, pp. 579-584.

21. A. Abe and G. Marcu, Neural network approach for RGB to YMCK color conversion, *Proc. of the IEEE Region 10 9th Annual International Conference TENCON'94*, vol. 1, 1994, pp. 6-9.

22. J. Z. Chang, J. P. Allebach and C. A. Bouman, Sequential linear interpolation of multidimensional functions, *IEEE Transactions on Image Processing*, **6**, 1231-1245 (1997).

23. A. U. Agar and J. P. Allebach, A Minimax Method for Function Interpolation Using an SLI Structure', *Proceedings of the IEEE International Conference on Image Processing*, Santa Barbara, CA, 1997, pp. 671-674.